LANGMUIR

pubs.acs.org/Langmuir Article

Photochemical Oxidation of Polyethylene Terephthalate Microplastics Adsorbed on Sand and Silica Surfaces

Camila Q. V. Costa, Amir Nobahar,* Agata Egea-Corbacho, Steffen Jockusch, Deborah M. Power, Vaidhyanathan Ramamurthy, and José P. Da Silva*

Cite This: *Langmuir* 2024, 40, 21476−21483 Read Online

ACCESS | Metrics & More | Article Recommendations | Supporting Information

ABSTRACT: The environmental contamination by plastics, microplastics, and related compounds is a major concern. While the detection and release of micro- and nanoparticles from these materials have been widely studied, the formation and release of molecules resulting from their degradation in the environment have been overlooked. This work presents a study of the products released from poly(ethylene terephthalate) (PET) irradiated as pure particles and adsorbed on silica and sand surfaces under different irradiation conditions. The role of oxygen was also evaluated. The products were identified by gas chromatography-mass spectrometry (GC-MS) and liquid chromatography-high resolution mass spectrometry (LC-HRMS). The main released molecules can be accounted for by considering the cleavage of α- and β-bonds next to the ester moiety of the polymer chain. Volatile products such as benzene as well as monomer units of the polymer and related products were identified. In the presence of oxygen, acetic acid and products resulting from hydroxylation at the benzenic ring or at the ethyl moiety were detected. Adsorption on silica and sand has little effect on the photoproduct distributions. The irradiation at 360 nm leads to distributions similar to the ones observed at 257 nm, but the reaction rate is lower. The identified product ethylene terephthalate is a marker of PET plastics and particles and can therefore be used to evaluate the environmental contamination by this polymer material.

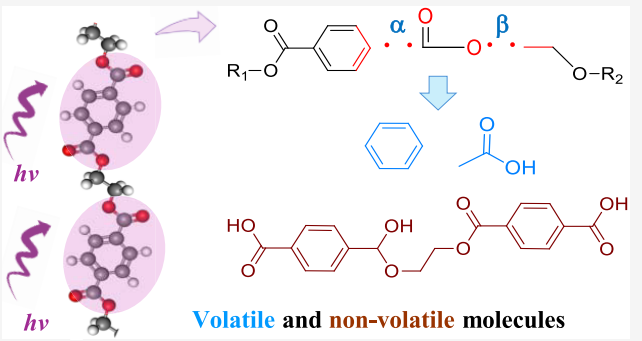

INTRODUCTION

Poly(ethylene terephthalate) (PET) is a thermoplastic with diverse applications in various industries due to its mechanical properties, transparency, and low cost. In 2022, the global PET consumption reached 25.47 million tons, and in 2030, it is forecasted to reach 35.70 million tons.[1] The increasing use of PET, namely, as bottles, clothing, and packaging, and improper postconsumer disposal have led to its accumulation in coastal and ocean ecosystems, where it undergoes transformation and contributes to environmental pollution.[2] PET degradation generates microplastic particles (<5 mm) that spread over the natural environment and can further degrade and release a variety of molecules that enter the food chain, threaten wildlife, and pollute the environment.[3]

It is known that the temperature of coastal areas and solar radiation lead to higher rates of plastic decomposition compared to the deep sea.[4] PET environmental photodegradation, which results from polymer exposure to the UV region of the solar spectrum at ground level, is recognized to be one of the most important abiotic degradation pathways of these materials.[5] PET absorbance was assigned to $\pi-\pi^*$ transitions localized on terephthalate moieties[6] that overlap with the solar spectrum in the region of 290−350 nm. Such overlap leads to direct degradation after sunlight absorbance.[7,8] The absorbance of UV radiation by the ester moiety results in the cleavage of C−C bonds in polymer, leading to radicals.[8] Diffuse reflectance laser flash photolysis studies of PET revealed the formation of multiple transients from the excited states of monomer, dimer, and excimer triplet states.[9] Furthermore, the reaction with atmospheric oxygen leads to the formation of an intermediate absorbing at 520 nm, which leads to photo-oxidation.

Despite significant research efforts, PET phototransformation is not fully understood, namely, the role of oxygen, the wavelength of irradiation,[10] and the effect of environmental conditions such as natural sand surfaces. However, it is known that PET chain scission during exposure to UV irradiation involves ester bond homolytic cleavage (Norrish type I α- and β-scissions) and Norrish type II hydrogen abstraction resulting

Received: June 17, 2024
Revised: September 20, 2024
Accepted: September 23, 2024
Published: October 1, 2024

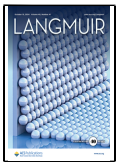

in carboxylic acid and vinyl end groups.[8,11] Furthermore, oxygen can influence the photolysis of PET by reacting with carbon-centered radicals formed during photolysis, which, in turn, could escalate the rate of polymer degradation.[12,13] Highly reactive oxygen species such as singlet oxygen or ozone may be formed, and these may further promote PET chain cleavage.[12,14] Most studies of PET photoreactions have focused on the changes in the surface chemistry after the reaction. Very few report the release and identification of final products.[8,11,14,16−18] Day and Wiles[11] reported the release of CO and CO_2 in vacuum photolysis and air photo-oxidation. Under ablative photodecomposition, besides CO and CO_2, hydrogen as well as benzene, toluene, and benzaldehyde are also released into the gas phase.[18] The presence of oxygen decreases the quantum yield of benzene formation under laser ablation conditions.[18] A recent study[17] reported the formation and release of oxygen-containing volatile compounds such as alcohols, aldehydes, ketones, and esters, as well as alkenes and alkanes, under low-pressure mercury arc lamp irradiation (365 and 254 nm) conditions. In addition, higher molecular weight PET oligomers, as well as carboxylic acids and other oxidized polymer fragments, were also detected.[15,16]

The toxicological evaluation indicated that some of the volatile and nonvolatile compounds released after photodegradation of PET pose toxic hazards to humans and the environment.[17,19−21] The present work further explores the problem generated by PET microparticles. The chosen matrix was a sand surface, a representative of marine coastal areas. Pure microparticles as well as silica-adsorbed particles were studied for comparison purposes. The results presented here summarize the array of degradation products formed, the role of oxygen, and the possible reaction pathways.

MATERIALS AND METHODS

Materials. Benzoic acid, terephthalic acid, PET, silica, and standard sand were from Sigma-Aldrich. Ethylene terephthalate (4,4′-((ethane−1,2-diylbis(oxy))bis(carbonyl))dibenzoic acid) was from BLDpharm. LC-MS grade water, methanol, and acetonitrile were purchased from Carlo Erba. Water for washing was obtained using a Milli-Q system (18 MΩ·cm). PET particles were prepared from granular PET using Cryo-MM400 cryogenic sample grinding equipment. The grinding process was performed at 30 rpm for 1 min per cycle, and a total of 6 cycles were conducted. Particles with sizes between 63 and 100 μm were sieved (CISA sieves) and used.

Sample Preparation. This study used the prepared pure PET microplastic and PET particles adsorbed on the surfaces of silica, standard sand, and natural sand. The solid matrices as well as the samples were prepared as described previously.[22] The natural sand used to adsorb microplastics was collected from the intertidal zone of Faro Island, coordinates 37.00747; −7.99485. Natural sand was sieved (45−50 mesh) and then washed with Milli-Q water. Before adsorption of microplastics, all surfaces were baked at 100 °C for 12 h to eliminate adsorbed contaminants.

PET particles were adsorbed on surfaces by using dichloromethane (DCM) as the solvent. The particles were added to a known amount of solid matrix to obtain a content of 1, 5, and 10 mg/g. DCM was then added to cover the solid surface mixed with the particles (1, 2, and 2 mL/g) in 20 mL vials. The vials were then closed, and the mixture was gently stirred for 30 min. Vials were then opened, and the solvent was evaporated at room temperature with continuous gentle stirring. The samples were finally subjected to a thermal treatment at 70 °C for 40 min to remove the traces of DCM.

Photolysis of Pure and Adsorbed PET Particles. *Release of Nonvolatile Compounds.* PET particles were irradiated in the presence and absence of oxygen using a low-pressure mercury lamp (254 nm, 16 W, Applied Photophysics). In the former case, 50 mg of particles was spread on glass microscope slides. For product studies, the particles were positioned 1 cm from the lamp surface and were irradiated for 24 h. For the kinetic studies, particles (10 mg spread over ∼1 cm^2) were positioned at 3 cm from the lamp surface and irradiated for 3, 15, 24, 53, 77, and 108 h. The irradiated particles were then extracted with methanol and analyzed by LC-HRMS. Control samples, which were stored at room temperature in darkness, were submitted to the same analytical procedures for comparison purposes. Irradiations under a nitrogen atmosphere (absence of oxygen) were performed by placing the PET particles inside a quartz container. The nitrogen atmosphere was achieved by gently flowing pure nitrogen (99.99%) over the particles (50 mg) inside the container for an hour. The container was then sealed and exposed to UV radiation for 24 h. The effect of the irradiation wavelength was studied using two sets of lamps fitted in an LZC−4 V photoreactor from Luzchem. Irradiations were made using a set of 14 8W LZC-UVC (254 nm) lamps and a set of 14 8W LZC−367 UVA lamps (maximum 367 nm, range 315−400 nm, fwhm = 15 nm) for 24 h and 5 days. Twenty milligrams of PET particles was spread on a glass microscope slide over an area of ∼2 cm^2, and the sample was placed in the center of the photoreactor on a rotating turntable to achieve homogeneous irradiation. After irradiation, the samples were collected, extracted with 0.5 mL of methanol, filtrated using 13 mm PTFE syringe filters of 0.22 μm, and analyzed by LC-HRMS. The nonvolatile compounds released by particles of PET adsorbed at 1.0, 2.0, and 10.0 mg/g loadings were analyzed as described above, but 500 mg of samples was used and the extraction was performed with 1 mL for sand-adsorbed PET and 2 mL for silica-adsorbed PET.

Release of Volatile Compounds. The irradiations to analyze the volatile compounds, either under an air or nitrogen atmosphere, were performed inside a sealed cylindrical quartz container. In this case, a mercury arc lamp (Applied Photophysics, 400 W) was employed. This irradiation source is more powerful and therefore expected to give higher release rates of volatile compounds, enabling their detection. At the end of the irradiation, an SPME fiber was carefully inserted into the quartz container to collect the gas-phase compounds. After 10 min, the fiber was recoiled, and the adsorbed compounds were analyzed by manual SPME-GC-MS. The samples were placed at a distance of 10 cm from the lamp, and a water filter was placed in between to reduce heating. The volatile compounds released under nitrogen atmosphere were collected as described above, but the particles were submitted to a gentle flow of pure nitrogen (99.99%) for 1 h before irradiation. The volatile compounds released by PET particles adsorbed on the studied surfaces were determined as described above, but 500 mg of sample was used.

Analytical Methods. *LC-HRMS.* Methanol extracts obtained from the various samples before and after irradiation were analyzed by LC-HRMS. The chromatographic separation was performed on a Thermo Scientific ultimate 3000 UHPLC. A Thermo Scientific Accucore RP−18 (2.1 × 100 mm^2, 2.6 μm) column and water (A)/methanol or acetonitrile (B) mobile phase, all solvents containing 0.1% of formic acid, were used under APCI and ESI ionization. The gradient (in v/v %) started with 20% B for 1 min. Then, B increased linearly to 60% in 7 min and then to 100% B in an additional 14 min. This composition was maintained for 6 min. The mobile phase was returned to 20% of B in 1 min, and this composition was maintained for 4 min before the next run. The same program was used under ESI, but B was acetonitrile with 0.1% formic acid. The flow rate was 0.3 mL/min. The injection volume was 10 μL.

Mass analysis was performed on an Orbitrap Elite (Thermo Scientific) mass spectrometer equipped with APCI and ESI sources. Data were acquired under positive and negative polarities. Under APCI, the main ionization parameters were the following: vaporizer temperature of 380 °C; sheath gas flow of 30 arbitrary units; auxiliary gas flow of 20 arbitrary units; capillary temperature of 350 °C; source current of 5 μA; S-Lenses RF level of 69%. Under ESI, the parameters were as follows: heater temperature of 350 °C; sheath gas flow of 35 arbitrary units; auxiliary gas flow of 5 arbitrary units; capillary temperature of 350 °C; spray voltage of 3.2 kV; S-Lenses RF level of 69%. The scan range was 100−1500 m/z.

https://doi.org/10.1021/acs.langmuir.4c02281
Langmuir 2024, 40, 21476−21483

Scheme 1. Main Photoreaction Pathways and Some Potential Products from PET Microplastic Photodegradation

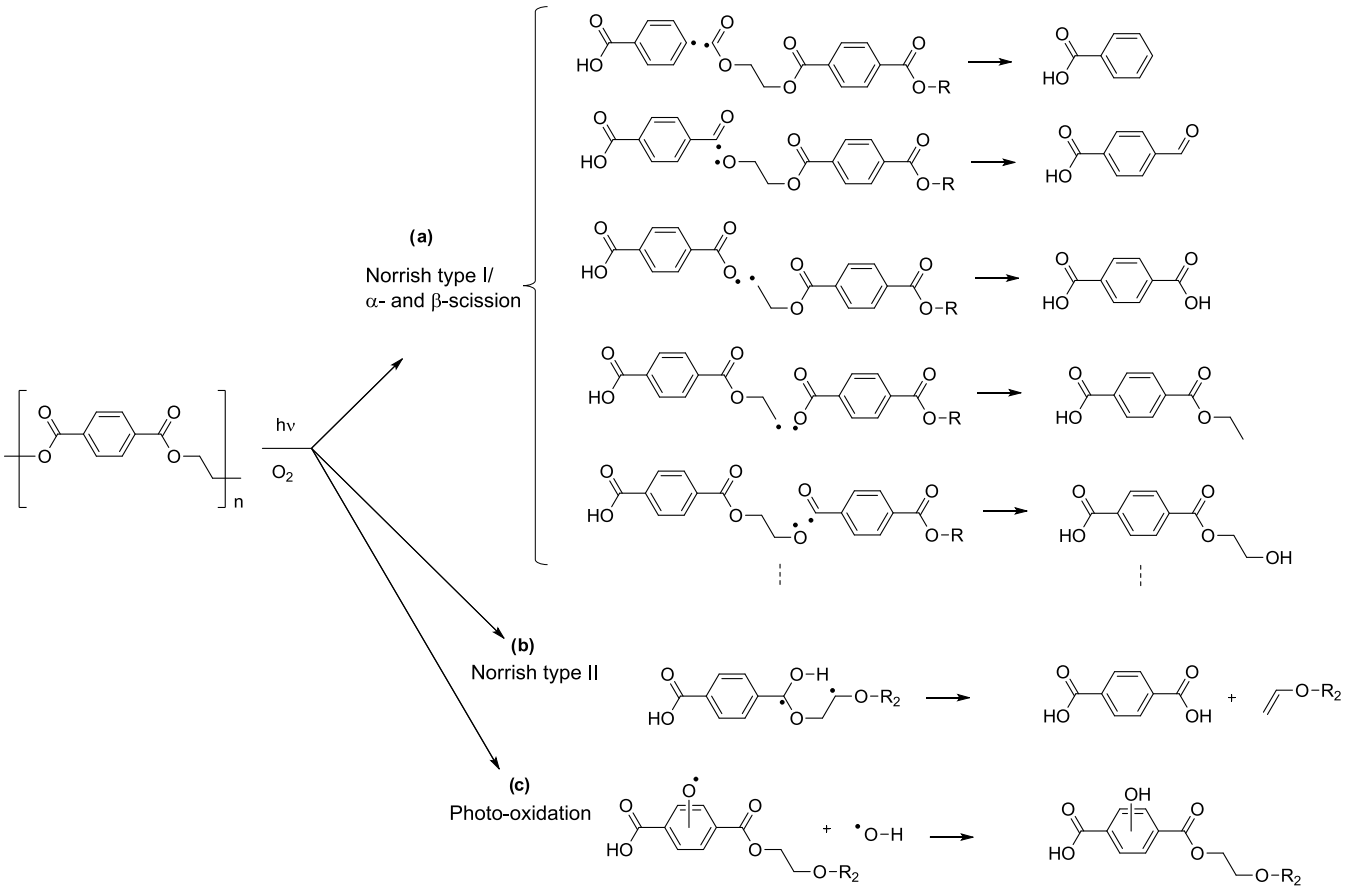

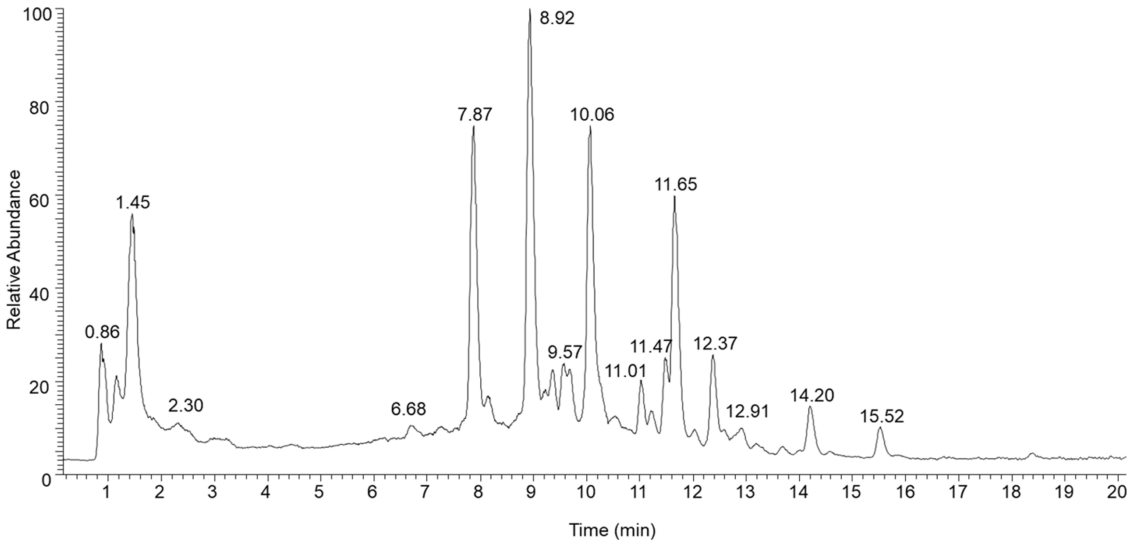

Figure 1. LC-HRMS full scan profile of a methanol extract of pure PET microplastic, obtained after 24 h of irradiation. Hg lamp, 16 W, negative ESI.

The samples were analyzed in full scan and data-dependent mode. Data-dependent analysis was achieved by selecting the three most intense ions under dynamic exclusion and collision-induced dissociation (CID) activation. LC-HRMS data analysis was performed using Xcalibur v. 4.1. Data-dependent profiles were processed using Compound Discoverer 3.3 (Thermo Fisher Scientific) to annotate the main signals. Profiles were processed using workflows for identification that include access to local and online databases such as mzCloud and Extractables and Leachables HRAM.

Quantification was performed by preparing calibration curves for selected standards and comparing the areas with those obtained from the samples. Areas were calculated after the integration of signals obtained using accurate mass-extracted ion chromatograms (AM-XIC, ± 5 ppm) taken from the full scan profiles (ESI ionization). Instrument limits of quantification of selected compounds were ∼1 ng/mL. The calibration range was between 20 and 800 ng/mL.

GC-MS. Volatile compounds were analyzed by SPME-GC-MS after irradiating the samples as described above. Resulting gaseous products

https://doi.org/10.1021/acs.langmuir.4c02281
Langmuir 2024, 40, 21476−21483

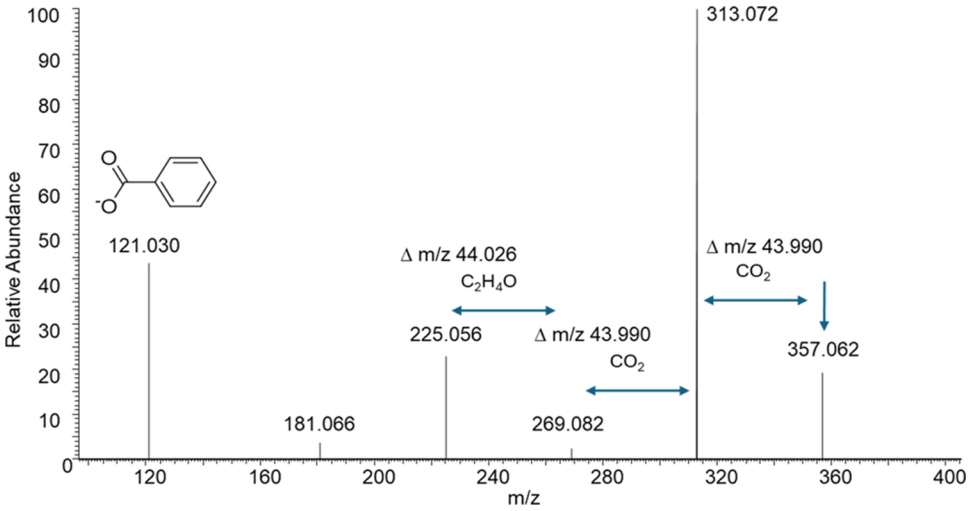

Figure 2. CID spectrum of photoproduct with m/z 357.062. Infusion, negative ESI.

were adsorbed on the fiber at room temperature over a period of 10 min and then desorbed after insertion of the fiber into the injection port liner, which was set at 280 °C. Analyses were conducted on a Bruker Scion TQ GC-MS using a DB−5 column (30 m long, 0.25 mm inner diameter, 0.25 μm film thickness). The temperature program started at 40 °C. The initial temperature was maintained for 2 min, then raised to 10 °C/min up to 280 °C, and held at this temperature for an additional 5 min. The solvent delay was 2.5 min. Analysis was also performed without solvent delay to detect compounds with very low retention times. In this case, the temperature ramp rate was 5 °C/min. The annotation of compounds was performed using the NIST (2014, 10th ed) library.

RESULTS AND DISCUSSION

Main Photoproducts. The profiles obtained under data-dependent acquisition (LC-HRMS^2) were analyzed using Compound Discoverer 3.3, and the main signals were annotated. Standards of selected annotated compounds were further analyzed to confirm their identity. Identification denotes the compounds analyzed in the extracts that possessed parameters, namely, retention time, exact masses, isotope distributions, and fragmentation patterns, identical to standards analyzed under the same conditions, while annotation is the evaluation of the spectral similarity between the gathered experimental data and those of public or commercial libraries. Additionally, putatively characterized compound classes were those that had signals showing spectral data consistent with a particular class of organic compounds.[23]

From mechanistic information available in the literature,[8,11] the main compounds are expected to possess carboxylic acid moieties, and therefore, ionization under negative ESI should be the most sensitive. Our approach to evaluate the different reaction processes under different conditions was to search for molecules possessing one benzoic acid moiety at one end and formed after Norrish type I/α- and β-scission, Norrish type II and photo/oxidation reactions, or combinations thereof (see Scheme 1 above). These products were searched in the LC-HRMS profiles by extracting their AM-XIC using a ± 5 ppm window.

We started by identifying and annotating the main products detected under negative ESI. Figure 1 presents a typical LC-HRMS full scan profile showing 5 main signals under negative ESI. The peak observed at 1.45 min was assigned to benzoic acid and terephthalic acid (which have overlapping peaks under our conditions) and confirmed after the analysis of the corresponding standards. As no match was found in mass spectral libraries for the compound observed at 7.87 min (m/z 357.062), further mass spectrometry studies were performed. The MS^2 spectra (Figure 2) of m/z 357.062 showed that the reaction involved the loss of CO_2. The high mass accuracy allowed us to distinguish between the loss of CO_2 (43.990 Da) and the loss of C_2H_4O (44.026 Da). However, the formation of the signal at m/z 225.056 cannot be explained by simple cleavage of the signal at m/z 357.062. After the first CO_2 is lost (spectrum of Figure 2), the fragmentation of m/z 313.072 (spectrum a, Figure S1) needs a release of $C_3H_4O_3$ while keeping the benzenic moieties together. The observation of m/z 225.056 could be rationalized assuming the terephthalic rings are bent over each other in the gas phase, and this allows neutral losses involving the oxyethylene moiety. Based on the mass spectral properties, the compound was initially assigned to ethylene terephthalate (4,4′-((ethane−1,2-diylbis(oxy))bis-(carbonyl))dibenzoic acid), and this was confirmed using a standard (see Table S1). The formation of terephthalic acid and ethylene terephthalate from PET photodegradation over time indicates that these compounds undergo a secondary photoreaction (Figure S2, Supporting Information).

The same studies were performed on the product in Figure 1 with a retention time of 8.92 min (m/z = 385.093). In common with m/z 357.062, the CID fragmentation of this signal leads to m/z 341.103 after release of CO_2 (Figure S3, SI). The difference from the compound with m/z 357.062 was observed after further fragmentation of the ion (m/z 341.103) and the signal at m/z 297.077, which showed the presence of two C_2H_4 units. However, the signal at m/z 225.056 was present in both compounds (m/z 385.093 and m/z 357.062). We propose this structure to be an analogue of ethylene terephthalate possessing an ethoxycarbonyl group replacing a carboxyl moiety end group (see Table S1). Figure S4 (SI) shows the fragmentation spectra of both compounds (m/z = 357.062 and 385.093) under HCD, which allows the detection of ions with lower m/z values and can potentially give new insights into the molecular structure of ions. The same main daughter ions detected under CID were observed, but the signals observed at m/z 121.030 and 181.066 under HCD show higher relative intensity.

https://doi.org/10.1021/acs.langmuir.4c02281
Langmuir 2024, 40, 21476−21483

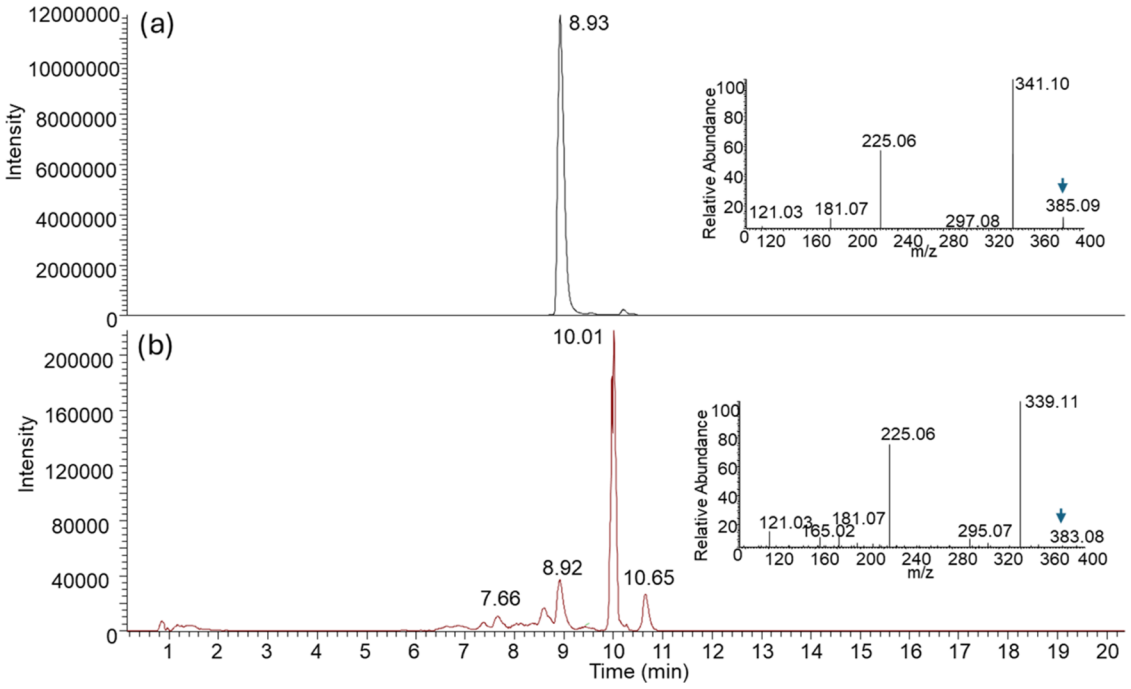

Figure 3. Accurate mass-extracted ion chromatograms (±5 ppm) taken from full scan LC-HRMS profiles of a methanol extract of PET microplastic obtained after 24 h irradiation. (a) 385.093, product formed after β-cleavage; (b) 383.077, product formed after Norrish type II and β-cleavage. The insets show the fragmentation spectra of compounds with m/z 385.09 (in a) and 383.08 (in b). Hg lamp, 16 W, negative ESI.

Similar studies were made for the products in Figure 2 with retention times of 10.06 min (m/z 549.104) and 11.65 min (m/z 605.166). Figure S5 shows the CID spectra as well as the HCD spectra of both compounds. CID spectra revealed the formation of m/z 357.062 and 385.093 after fragmentation of m/z 549.104 and m/z 605.166, respectively, while HCD revealed the formation of benzoic acid and terephthalic acid anions, suggesting that these compounds are analogues of compounds detected at m/z 357.052 and 385.093 containing one more PET monomer. All of the main products mentioned above can be accounted for by α- and β-scission of the ester moiety or Norrish type II reactions (Scheme 1a,b).

It should be noted that the detected major photoproducts were already present in PET particles before the reaction. These compounds might have been formed during the synthesis and/or polymer processing.[24] Furthermore, during synthesis, PET is subjected to temperatures between 200 and 300 °C that can lead to the degradation of the polymer.[8] However, irradiation of PET in our study increased the intensities of the main products by about 50 times (Figure S6, SI).

The formation of PET oligomers was reported after irradiation of PET films[16] while terephthalic acid and other oxidized PET fragments were tentatively identified after photoreaction of PET particles in Milli-Q water suspensions.[15]

Other Photoproducts. We searched for other products formed after Norrish type I/α- and β-scission by considering the reactions presented in Scheme 1a and extracting the corresponding exact mass of each compound from the LC-HRMS full scan profiles using a ±5 ppm window. See the list of compounds in Scheme S1 in SI.

All ions of the postulated compounds were found in the methanol extracts of irradiated PET particles (Hg lamp, 16 W, 24 h). Some of them showed a single major signal, while others showed more than one chromatographic peak, indicating the presence of isomers (see Figure S7 for an example). The additional compounds observed at m/z 401.088, for example, may be hydroxylation products of a compound with m/z 385.093. The CID fragmentation of larger oligomers released the ions of the main detected compounds, namely, the ions with m/z 357.062 and 385.093, indicating that they were analogues of these two major photoproducts.

A Norrish type II mechanism leading to β-scission of the 1,4-diradical, on the other hand, leads to the formation of vinyl end groups (see Scheme 1b), which can also be searched in the products' profiles (Scheme S2, SI) by following the same approach (AM-XIC). Figure S8 shows the fragmentation spectra of a compound possessing a vinyl group (m/z 383.077) and the corresponding compound but with the ethyl moiety (m/z 385.093), supporting the assignments. The comparison of the chromatographic signals of these two compounds showed that the intensity of the one with m/z 383.077 is at least 50 times lower (Figure 3). The same comparison for products with m/z 193.051 and 191.035 revealed that the product formed after Norrish type II still had lower intensities but was half of the one formed by α-/β-cleavage (Figure S9, SI). Other annotated and characterized compounds detected under negative ESI are listed in Table S1, SI file.

Positive ESI is sensitive to compounds without a carboxylic acid moiety such as a benzaldehyde group (see Scheme S3, SI). Some products with a benzaldehyde end group formed after a Norrish type I reaction are listed in Scheme S3 (SI). Most postulated products were not detected. Signals at m/z 327.086, 387.107, and 683.176 were however detected, but there was no clear relationship between the postulated structures and the fragmentation spectra.

Volatile Compounds. The main volatile compounds were studied by SPME-GC-MS, which allowed for the collection of gaseous products in the atmosphere above the surface of PET-irradiated particles. The main detected compounds were acetic

https://doi.org/10.1021/acs.langmuir.4c02281
Langmuir 2024, 40, 21476−21483

Scheme 2. Main Reaction Pathways and Products Found for PET Microplastic

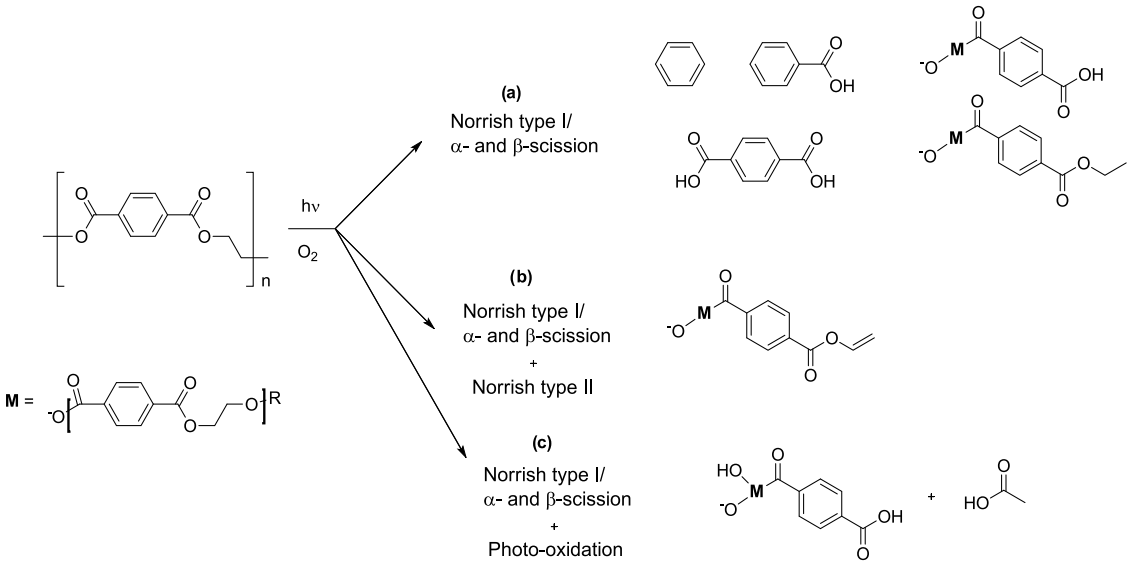

acid, acetone, and benzene (Table S2, SI). The photorelease of benzene from PET has been reported under laser ablation conditions of PET.[18] The release of acetone was reported after thermal degradation of PET.[25] However, acetic acid, as far as we know, has not been reported.

Role of Oxygen and Irradiation Wavelength. Both volatile and nonvolatile compounds were studied in the presence and absence of oxygen. Under nitrogen a atmosphere, the release of benzene increased relative to an air atmosphere, in agreement with results observed under laser ablation,[18] while the formation of acetic acid decreased (see Figure S10). The formation of aliphatic carboxylic acids resulting from the photoreaction of PET has not been reported, probably because most studies are performed by GC-MS and carboxylic acids are difficult to detect under the analytical conditions generally used, as shown in Figure S10 where acetic acid shows a broad chromatographic peak. The analyses of these compounds by GC-MS usually require a derivatization reaction such as esterification, which is not feasible under SPME sampling. However, results obtained from LC-HRMS confirmed the presence of other small aliphatic carboxylic acids such as succinic acid, besides acetic acid (Table S1, Figure S11, SI). The yield of the acids decreased in the absence of oxygen. In general, the presence of oxygen increased the yields of the major degradation products (Figure S12, SI).

The formation of hydroxylated products of PET can be explained by the formation of hydroperoxides[8] and is therefore associated with the presence of oxygen. We searched the LC-HRMS profiles for the hydroxylated compounds considered in the reactions a−c of Scheme 1. Scheme S4, SI, lists the compounds examined. Figure S13 shows a comparison of the hydroxylated product of ethylene terephthalate (m/z = 373.057) obtained after irradiation in air and nitrogen atmospheres. The signals increased 20-fold in the presence of oxygen. Furthermore, at least two isomers were formed, suggesting that hydroxylation occurred at more than one site. All exact masses of postulated hydroxylated compounds (Scheme S4, SI) were detected and increased in the presence of oxygen.

Photoproduct distributions of the main products obtained after irradiation with UVC lamps (254 nm) and UVA lamps (315−367 nm) and a 16 W Hg lamp were similar, but the reaction rate under UVA was much lower (Figure S14). Lower rates are expected under UVA as the absorbance of PET is much lower under these conditions.[26]

Surface Effect on PET Photodegradation. The photo-oxidation of PET particles was also studied when they were adsorbed on silica, standard sand, and natural sand surfaces. Figure S15 presents the profiles of the main photoproducts released by irradiated pure particles and particles adsorbed on each of these surfaces. As observed for other microplastic materials,[22] no significant effect of the nature of the surface on the photoproduct distributions was detected. These results indicate that the same products are released from PET materials and particles adsorbed on natural inorganic surfaces, such as beach sand. As expected, the amounts of products released after the same irradiation time increased with the loading (Figure S16). However, the distribution of the products had a similar pattern.

Main Reaction Pathways. Esters can undergo α-cleavage of the (O═)C−O bond or the C−C(═O) bond on irradiation or alternatively β-cleavage of the O−C bond, which often leads to decarboxylation.[27] While α- and β-scissions generate radicals at the ester moiety, the Norrish type II mechanism generates a radical pair involving intramolecular hydrogen abstraction in a six-member ring transition state, which is expected to take place in the amorphous regions of the polymer.[11] The formed radicals can recombine, undergo further cleavage, release products such as CO and CO_2, abstract hydrogen, and propagate the reaction or undergo cross-linking. In the presence of oxygen, hydroperoxides (POOH) can be formed[22] leading to polymer oxy and hydroxyl radicals (PO• and •OH), which can further react with the polymer.

The main reaction products detected by LC-HRMS are either aromatic acids or possess at least one aromatic acid end-group. Key products are presented in Scheme 2. These products are formed even under a nitrogen atmosphere, meaning the aromatic carboxylic acid moieties were not generated from molecular oxygen and were therefore produced after the reaction of the polymer chain only. These products can be readily accounted for by α- and β-scissions of the ester

https://doi.org/10.1021/acs.langmuir.4c02281
Langmuir 2024, 40, 21476−21483

groups, followed by hydrogen abstraction (Scheme 2, reaction a). The observed release of benzene detected by SPME-GC-MS is in line with the release of CO and CO_2 and can be explained by further homolytic cleavage of the formed primary radicals, followed by hydrogen abstraction.

The presence of vinyl a moiety is an indication of the Norrish type II reaction, which also takes place. However, the comparison between the intensity of signals of these products and the corresponding products formed after α- and β-scissions indicates their yields are significantly lower (Figures 2 and S9, SI). As vinyl groups are more reactive toward oxygen than carbonyl and carboxylic groups,[8] we compared the contents of the Norrish type II product with m/z 383.077 in the presence and absence of oxygen to evaluate whether these products underwent secondary photoreaction, but the intensities observed in both conditions (presence and absence of oxygen) were similar. The results suggest that the Norrish type II reaction was a minor reaction, and this can be explained by restrictions in the molecular motion to form the transition state in the solid state. The relative increase in the Norrish type II products for lower molecular weight compounds (Figures 2 and S9) can be explained by reactions at the end of the polymer chain and/or secondary photoreaction of polymer oligomers, where the formation of the transition state that gives rise to the radical pair is facilitated.

The formation of acetic acid indicates that photo-oxidation takes place at the ethyl moiety. The decrease in the release of benzene in the presence of oxygen may be due to a less efficient decarboxylation from polymer oxy radicals and/or the reaction of the formed benzene radicals with molecular oxygen to form phenyl peroxy radicals. Signals for hydroxylated analogues of products formed after α- and β-scission, such as hydroxy benzoic acid, were detected (Scheme S4), suggesting that hydroxylation was also taking place at the aromatic ring. Mechanisms might involve the formation and cleavage of hydroperoxides and/or hydroxy radicals attached to the aromatic rings.[8]

CONCLUSIONS

The photoreaction of PET microplastic can be readily explained by considering that the polymer undergoes α- and β-cleavage at the ester moiety, leading to the formation of radicals that after reaction release diverse products reflecting the position of the homolytic cleavages of the involved bonds. The main products included polymer monomers and related compounds as well as oligomers. Norrish type II reaction products were detected, but their yields were significantly lower, and this was associated with constraints in the formation of the transition state that leads to the radical pair. The presence of oxygen led to hydroxylation at the benzene and/or ethyl moiety. A similar distribution of products was observed for pure particles and PET particles adsorbed on silica or sand. The irradiation at longer wavelengths (367 nm) formed the same products observed at 254 nm. Therefore, the detected compounds are likely to be released from PET plastics and microplastics under natural conditions and on inorganic surfaces, such as beach sand. Ethylene terephthalate is uniquely related to the structure of PET and therefore can be used as an environmental marker to assess the contamination by these polymer materials.

ASSOCIATED CONTENT

Supporting Information

The Supporting Information is available free of charge at https://pubs.acs.org/doi/10.1021/acs.langmuir.4c02281.

Schemes S1−S4 present reaction mechanisms and the associated/expected photoproducts. Tables S1 and S2 list the products annotated/identified that are released from PET particles. Figures S1−S16 show mass spectra; amounts of products formed over time; and various LC-HRMS profiles of pure and adsorbed PET particles of selected sample sets (PDF)

AUTHOR INFORMATION

Corresponding Authors

Amir Nobahar − *Centre of Marine Sciences (CCMAR/CIMAR LA), University of Algarve, Campus de Gambelas, Faro 8005-139, Portugal;* orcid.org/0000-0002-7401-9076; Email: nobahar.amir@gmail.com

José P. Da Silva − *Centre of Marine Sciences (CCMAR/CIMAR LA), University of Algarve, Campus de Gambelas, Faro 8005-139, Portugal;* orcid.org/0000-0002-6458-7328; Email: jpsilva@ualg.pt

Authors

Camila Q. V. Costa − *Centre of Marine Sciences (CCMAR/CIMAR LA), University of Algarve, Campus de Gambelas, Faro 8005-139, Portugal*

Agata Egea-Corbacho − *Department of Environmental Technologies, Faculty of Marine and Environmental Sciences, University of Cadiz, Puerto Real, Cádiz 11510, Spain*

Steffen Jockusch − *Center for Photochemical Sciences, Bowling Green State University, Bowling Green, Ohio 43403, United States;* orcid.org/0000-0002-4592-5280

Deborah M. Power − *Centre of Marine Sciences (CCMAR/CIMAR LA), University of Algarve, Campus de Gambelas, Faro 8005-139, Portugal;* orcid.org/0000-0003-1366-0246

Vaidhyanathan Ramamurthy − *Department of Chemistry, University of Miami, Coral Gables, Florida 33146, United States;* orcid.org/0000-0002-3168-2185

Complete contact information is available at: https://pubs.acs.org/10.1021/acs.langmuir.4c02281

Author Contributions

The manuscript was written through the contributions of all authors. All authors have given their approval to the final version of the manuscript.

Funding

Portuguese FCT-Foundation for Science and Technology, projects EXPL/CTA-AMB/1613/2021 (DOI: 10.54499/EXPL/CTA-AMB/1613/2021), UIDB/04326/2020 (DOI:10.54499/UIDB/04326/2020), UIDP/04326/2020 (DOI:10.54499/UIDP/04326/2020) and LA/P/0101/2020 (DOI:10.54499/LA/P/0101/2020), and grant 2022.14374.BD. Operational programmes CRESC Algarve 2020 and COMPETE 2020, grant EMBRC.PT ALG-01−0145-FEDER-022121.

Notes

The authors declare no competing financial interest.

■ ACKNOWLEDGMENTS

C.Q.V.C. thanks FCT grant 2022.14374.BD. This study received Portuguese national funds from FCT-Foundation for Science and Technology through projects EXPL/CTA-AMB/1613/2021 (DOI: 10.54499/EXPL/CTA-AMB/1613/2021), UIDB/04326/2020 (DOI:10.54499/UIDB/04326/2020), UIDP/04326/2020 (DOI:10.54499/UIDP/04326/2020), and LA/P/0101/2020 (DOI:10.54499/LA/P/0101/2020) and from the operational programmes CRESC Algarve 2020 and COMPETE 2020 through project EMBRC.PT ALG-01-0145-FEDER-022121.

■ ABBREVIATIONS

PET, poly(ethylene terephthalate); SPME-GC-MS, solid phase micro extraction−gas chromatography−mass spectrometry; LC-HRMS, liquid chromatography coupled to high-resolution mass spectrometry

■ REFERENCES

(1) Statista. Market volume of polyethylene terephthalate worldwide from 2015 to 2022, with a forecast for 2023 to 2030. https://www.statista.com/statistics/1245264/polyethylene-terephthalate-market-volume-worldwide/. (accessed June 17, 2024).

(2) Dhaka, V.; Singh, S.; Anil, A. G.; Naik, T. S. S. K.; Garg, S.; Samuel, J.; Kumar, M.; Ramamurthy, P. C.; Singh, J. Occurrence, Toxicity and Remediation of Polyethylene Terephthalate Plastics. A Review. *Environ. Chem. Lett.* **2022**, *20*, 1777−1800.

(3) Rose, P. K.; Yadav, S.; Kataria, N.; Khoo, K. S. Microplastics and Nanoplastics in the Terrestrial Food Chain: Uptake, Translocation, Trophic Transfer, Ecotoxicology, and Human Health Risk. *TrAC, Trends Anal. Chem.* **2023**, *167*, No. 117249.

(4) Barboza, L. G. A.; Cózar, A.; Gimenez, B. C. G.; Barros, T. L.; Kershaw, P. J.; Guilhermino, L. Macroplastics Pollution in the Marine Environment. In *World Seas: An Environmental Evaluation*, 2nd ed.; Academic Press, 2019; pp 305−328.

(5) Sang, T.; Wallis, C. J.; Hill, G.; Britovsek, G. J. P. Polyethylene Terephthalate Degradation under Natural and Accelerated Weathering Conditions. *Eur. Polym. J.* **2020**, *136*, No. 109873.

(6) LaFemina, J. P.; Arjavalingam, G. Photophysics of Poly(Ethylene Terephthalate): Ultraviolet Absorption and Emission. *J. Phys. Chem. A* **1991**, *95*, 984−988.

(7) Fechine, G. J. M.; Rabello, M. S.; Souto Maior, R. M.; Catalani, L. H. Surface Characterization of Photodegraded Poly(Ethylene Terephthalate). The Effect of Ultraviolet Absorbers. *Polymer* **2004**, *45*, 2303−2308.

(8) Rabek, J. F. *Polymer Photodegradation*; Springer: Netherlands, 1995.

(9) Fukazawa, N.; Yoshioka, K.; Fukumura, H.; Masuhara, H. Diffuse Reflectance Laser Photolysis and Luminescence Study on Poly(Ethylene Terephthalate) Powder. *J. Phys. Chem. A* **1993**, *97*, 6753−6759.

(10) Ferreira, M. M.; da Silva, E. A.; Cotting, F.; Lins, V. de F. C. UV Weathering and Performance of a Novel Corrosion Protective Coating on Steel Made from Recycled Polyethylene Terephthalate (PET). *Corros. Eng. Sci. Technol.* **2021**, *56*, 199−209.

(11) Day, M.; Wiles, D. M. Photochemical Degradation of Poly(Ethylene Terephthalate). III. Determination of Decomposition Products and Reaction Mechanism. *J. Appl. Polym. Sci.* **1972**, *16*, 203−215.

(12) Lee, C. O.; Chae, B.; Kim, S. B.; Jung, Y. M.; Lee, S. W. Two-Dimensional Correlation Analysis Study of the Photo-Degradation of Poly(Ethylene Terephthalate) Film. *Vib. Spectrosc.* **2012**, *60*, 142−145.

(13) Fotopoulou, K. N.; Karapanagioti, H. K. Degradation of Various Plastics in the Environment. In *Hazardous Chemicals Associated with Plastics in the Marine Environment. The Handbook of Environmental Chemistry*; Springer: Cham, 2017; pp 71−92.

(14) Grossetête, T.; Rivaton, A.; Gardette, J. L.; Hoyle, C. E.; Ziemer, M.; Fagerburg, D. R.; Clauberg, H. Photochemical Degradation of Poly(Ethylene Terephthalate)-Modified Copolymer. *Polymer* **2000**, *41*, 3541−3554.

(15) Gewert, B.; Plassmann, M.; Sandblom, O.; Macleod, M. Identification of Chain Scission Products Released to Water by Plastic Exposed to Ultraviolet Light. *Environ. Sci. Technol. Lett.* **2018**, *5*, 272−276.

(16) Watanabe, R.; Sugahara, A.; Shinzawa, H.; Yamane, S.; Nakamura, S.; Sato, H.; Hagihara, H.; Oishi, A.; Mizukado, J.; Ueda, Y.; Satoh, T. Photodegradation Behavior of Polyethylene Terephthalate Analyzed by MALDI-TOFMS and ATR-FTIR Microscopic Analysis in Combination with Two-Trace Two-Dimensional (2T2D) Correlation Mapping. *Polym. Degrad. Stab.* **2023**, *208*, No. 110246.

(17) Wu, X.; Tan, Z.; Liu, R.; Liao, Z.; Ou, H. Gaseous Products Generated from Polyethylene and Polyethylene Terephthalate during Ultraviolet Irradiation: Mechanism, Pathway and Toxicological Analyses. *Sci. Total Environ.* **2023**, *876*, No. 162717.

(18) Srinivasan, R.; Leigh, W. J. Ablative Photodecomposition: Action of Far-Ultraviolet (193 Nm) Laser Radiation on Poly(Ethylene Terephthalate) Films. *J. Am. Chem. Soc.* **1982**, *104*, 6784−6785.

(19) Lee, J.; Pedersen, A. B.; Thomsen, M. The Influence of Resource Strategies on Childhood Phthalate Exposure-The Role of REACH in a Zero Waste Society. *Environ. Int.* **2014**, *73*, 312−322.

(20) Djapovic, M.; Milivojevic, D.; Ilic-Tomic, T.; Lješević, M.; Nikolaivits, E.; Topakas, E.; Maslak, V.; Nikodinovic-Runic, J. Synthesis and Characterization of Polyethylene Terephthalate (PET) Precursors and Potential Degradation Products: Toxicity Study and Application in Discovery of Novel PETases. *Chemosphere* **2021**, *275*, No. 130005.

(21) Klein, K.; Hof, D.; Dombrowski, A.; Schweyen, P.; Dierkes, G.; Ternes, T.; Schulte-Oehlmann, U.; Oehlmann, J. Enhanced in Vitro Toxicity of Plastic Leachates after UV Irradiation. *Water Res.* **2021**, *199*, No. 117203.

(22) Costa, C. Q. V.; Afonso, I. I.; Cruz, J.; Teodósio, M. A. A.; Jockusch, S.; Ramamurthy, V.; Power, D. M.; Da Silva, J. P. Environmental Markers of Plastics and Microplastics. *Environ. Sci. Technol.* **2024**, *58*, 8889−8898.

(23) Viant, M. R.; Kurland, I. J.; Jones, M. R.; Dunn, W. B. How Close Are We to Complete Annotation of Metabolomes? *Curr. Opin. Chem. Biol.* **2017**, *36*, 64−69.

(24) Pang, K.; Kotek, R.; Tonelli, A. Review of Conventional and Novel Polymerization Processes for Polyesters. *Prog. Polym. Sci.* **2006**, *31*, 1009−1037.

(25) Abboudi, M.; Odeh, A.; Aljoumaa, K. Carbonyl Compound Leaching from Polyethylene Terephthalate into Bottled Water under Sunlight Exposure. *Toxicol. Environ. Chem.* **2016**, *98*, 167−178.

(26) Prasad, S. G.; De, A.; De, U. Structural and Optical Investigations of Radiation Damage in Transparent PET Polymer Films. *Int. J. Spectrosc.* **2011**, *2011*, No. 810936.

(27) Coyle, J. D. Photochemistry of Carboxylic Acid Derivatives. *Chem. Rev.* **1978**, *78*, 97−123.

https://doi.org/10.1021/acs.langmuir.4c02281
Langmuir 2024, 40, 21476−21483